On the prediction of equilibrium states in homogeneous turbulence

By CHARLES G. SPEZIALE
AND NESSAN MAC GIOLLA MHUIRIS†

Institute for Computer Applications in Science and Engineering, NASA Langley Research Center, Hampton, VA 23665, USA

A comparison of several commonly used turbulence models (including the K–ϵ model and three second-order closures) is made for the test problem of homogeneous turbulent shear flow in a rotating frame. The time evolution of the turbulent kinetic energy and dissipation rate is calculated for these models and comparisons are made with previously published experiments and numerical simulations. Particular emphasis is placed on examining the ability of each model to predict equilibrium states accurately for a range of the parameter Ω/S (the ratio of the rotation rate to the shear rate). It is found that none of the commonly used second-order closure models yield substantially improved predictions for the time evolution of the turbulent kinetic energy and dissipation rate over the somewhat defective results obtained from the simpler K–ϵ model for the unstable flow regime. There is also a problem with the equilibrium states predicted by the various models. For example, the K–ϵ model erroneously yields equilibrium states that are independent of Ω/S while the Launder, Reece & Rodi model and the Shih–Lumley model predict a flow relaminarization when $\Omega/S > 0.39$ – a result that is contrary to numerical simulations and linear spectral analyses, which indicate flow instability for at least the range $0 \leqslant \Omega/S \leqslant 0.5$. The physical implications of the results obtained from the various turbulence models considered herein are discussed in detail along with proposals to remedy the deficiencies based on a dynamical systems approach.

1. Introduction

Homogeneous turbulent flows have played a central role in the calibration and testing of a variety of turbulence models. The reason for this prominence is twofold: (*a*) homogeneous turbulence contains many of the important flow effects of scientific and engineering interest in a simplified setting which quite often gives rise to closed-form solutions in the commonly used turbulence models, and (*b*) there is an abundance of reliable data from physical and numerical experiments with which to compare the predictions of turbulence models. In particular, the physical and numerical experiments on homogeneous plane shear and plane strain (see Tucker & Reynolds 1968; Champagne, Harris & Corrsin 1970; Tavoularis & Corrsin 1981; Rogallo 1981) have been used extensively in the calibration of second-order closure models and the most recent two-equation models of the K–ϵ type. When a two-

† Present address: Mathematics Department, Case Western Reserve University, Cleveland, OH 44106, USA.

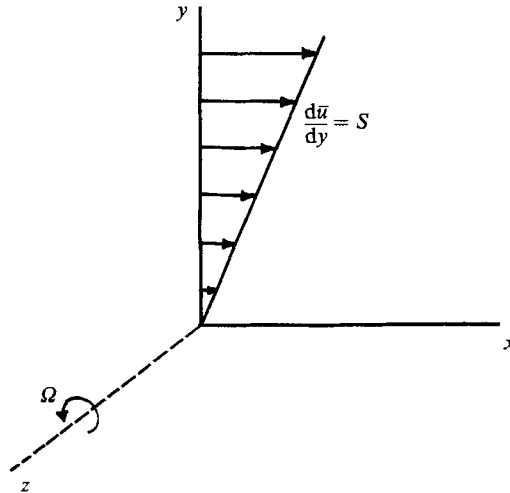$$\frac{\mathrm{d}\bar{u}}{\mathrm{d}y} = S$$

FIGURE 1. Homogeneous turbulent shear flow in a rotating frame.

equation turbulence model or a second-order closure model is applied to homogeneous turbulence, it gives rise to an initial-value problem for a set of coupled nonlinear ordinary differential equations – a dynamical systems problem. However, there appear to have been no previously published studies of homogeneous turbulence modelling from this nonlinear dynamics standpoint. This forms the motivation for the present study.

In this paper the performance of five commonly used turbulence models (the standard K–ϵ model, a nonlinear K–ϵ model, the Launder, Reece & Rodi second-order closure model, the Rotta–Kolmogorov second-order closure model and the Shih–Lumley second-order closure model) are examined for the test problem of homogeneous turbulent shear flow in a rotating frame. This problem constitutes a significant test since it encompasses arbitrary combinations of plane shear and plane rotation which can have either a stabilizing or destabilizing effect. The time evolution of the turbulent kinetic energy and dissipation rate will be computed along with equilibrium states which, mathematically, are the fixed points of the resulting system of nonlinear ordinary differential equations. Extensive comparisons with physical and numerical experiments will be made. The results obtained are somewhat disappointing, at least in a quantitative sense. For example, it will be shown that the commonly used two-equation models of the K–ϵ type yield predictions for the turbulent kinetic energy and dissipation rate that are independent of the state of rotation of the fluid – a result that is in substantial contradiction to numerical simulations of the Navier–Stokes equations. While the second-order closure models do yield rotationally dependent solutions, it will be shown that their predictions of the time evolution of the turbulent kinetic energy and dissipation rate are not (for the unstable flow regime where the kinetic energy and dissipation rate grow exponentially with time) substantially better than the simpler K–ϵ model. Considerable attention will be paid to the ability of each model to predict equilibrium states. In this regard, it will be shown that there are deficiencies in the commonly used second-order closures. For example, the Launder, Reece & Rodi model and the Shih–Lumley model will be shown to predict a flow relaminarization when $\Omega/S > 0.39$ whereas large-eddy simulations and linear spectral analyses indicate that

there is an exponential growth in the turbulent kinetic energy and dissipation rate for $0 \leqslant \Omega/S \leqslant 0.5$ (it is only their ratio, the turbulent timescale, that approaches a structural equilibrium). On the other hand, the K-ϵ model erroneously predicts unstable flow for all values of Ω/S with exactly the same turbulence structure. The results predicted by these five turbulence models will be documented in detail and specific proposals will be made for the development of improved models.

2. Turbulent shear flow in a rotating frame

We shall consider the problem of homogeneous turbulent shear flow in a steadily rotating frame for an incompressible viscous fluid (see figure 1). This problem is chosen because it incorporates arbitrary combinations of plane rotations and shear and, hence, represents a rather general class of homogeneous turbulent flows in a simplified setting. Since the homogeneous turbulence problem being considered is planar, the Reynolds equation is satisfied identically for all values of the rotation rate Ω and shear rate S (cf. Reynolds 1987). Consequently, no consistency problems can arise since the mean momentum and continuity equations are satisfied identically for the entire range of parameter space. For the problem at hand, the mean velocity gradient tensor in the rotating frame is given by

$$\frac{\partial \bar{v}_i}{\partial x_j} = \begin{pmatrix} 0 & S & 0 \\ 0 & 0 & 0 \\ 0 & 0 & 0 \end{pmatrix} \tag{1}$$

and $\Omega_i = (0,0,\Omega)$ denotes the rotation rate of the framing relative to an inertial frame of reference. We shall restrict our attention to incompressible fluids, with constant properties, for which the turbulence is initially isotropic.

First, we shall consider the traditional K-ϵ model for which the turbulent kinetic energy K and dissipation rate ϵ are solutions of the nonlinear ordinary differential equations (see Hanjalic & Launder 1972)

$$\dot{K} = \tau_{ij} \frac{\partial \bar{v}_i}{\partial x_j} - \epsilon, \tag{2}$$

$$\dot{\epsilon} = C_{\epsilon 1} \frac{\epsilon}{K} \tau_{ij} \frac{\partial \bar{v}_i}{\partial x_j} - C_{\epsilon 2} \frac{\epsilon^2}{K} \tag{3}$$

for any homogeneous turbulent flow. Here, τ_{ij} is the Reynolds stress tensor (such that $K = -\frac{1}{2}\tau_{ii}$) which is represented by the eddy viscosity model

$$\tau_{ij} = -\tfrac{2}{3}K\delta_{ij} + C_\mu \frac{K^2}{\epsilon}\left(\frac{\partial \bar{v}_i}{\partial x_j} + \frac{\partial \bar{v}_j}{\partial x_i}\right), \tag{4}$$

where C_μ, $C_{\epsilon 1}$ and $C_{\epsilon 2}$ are constants, which are usually taken to assume the values of 0.09, 1.45 and 1.90, respectively. For turbulent shear flow in a rotating frame, (2) and (3) simplify to

$$\dot{K} = C_\mu \frac{K^2}{\epsilon} S^2 - \epsilon, \tag{5}$$

$$\dot{\epsilon} = C_{\epsilon 1} C_\mu K S^2 - C_{\epsilon 2} \frac{\epsilon^2}{K}, \tag{6}$$

and the components of the anisotropy tensor $a_{ij} \equiv -(\tau_{ij}+\frac{2}{3}K\delta_{ij})/K$ are as follows:

$$a_{11} = 0, \quad a_{12} = -C_\mu SK/\epsilon, \quad a_{13} = 0, \tag{7}$$

$$a_{22} = 0, \quad a_{23} = 0, \quad a_{33} = 0. \tag{8}$$

Equations (5) and (6) can be combined to yield a nonlinear differential equation for ϵ/SK of the form

$$\frac{\mathrm{d}}{\mathrm{d}t^*}\left(\frac{\epsilon}{SK}\right) = C_\mu(C_{\epsilon 1}-1)-(C_{\epsilon 2}-1)\left(\frac{\epsilon}{SK}\right)^2, \tag{9}$$

where $t^* = St$ is the dimensionless time. The time evolution of the anisotropy tensor can be obtained from (7)–(9) which are solved subject to the initial condition

$$\frac{\epsilon}{SK} = \frac{\epsilon_0}{SK_0} \tag{10}$$

at time $t^* = 0$. Then, the turbulent kinetic energy can be obtained from (5) integrated in the form

$$\frac{\mathrm{d}K^*}{\mathrm{d}t^*} = \left(C_\mu\frac{SK}{\epsilon} - \frac{\epsilon}{SK}\right)K^*, \tag{11}$$

which constitutes a linear differential equation for $K^* \equiv K/K_0$ once ϵ/SK is determined from (9). Here, $\epsilon^* \equiv \epsilon/\epsilon_0$ can be easily obtained once K^* and ϵ/SK are known since

$$\epsilon^* = K^*\left(\frac{SK_0}{\epsilon_0}\right)\left(\frac{\epsilon}{SK}\right). \tag{12}$$

It therefore follows that the evolution of K^*, ϵ^* and SK/ϵ in dimensionless time t^* only depends on the shear rate and initial conditions through the dimensionless parameter SK_0/ϵ_0. Consequently, the K–ϵ model predicts that two homogeneous turbulent shear flows are dynamically similar provided that SK_0/ϵ_0 is the same for both flows. This is only partially consistent with the Navier–Stokes equations which at least require that both SK_0/ϵ_0 and the shape of the initial energy spectrum be the same for two flows to be dynamically similar. The equations of motion for the K–ϵ model in homogeneous turbulent shear flow are the same in all frames of reference independent of whether or not they are inertial and, therefore, the time evolution of K^*, ϵ^* and SK/ϵ are independent of the rotation rate Ω of the reference frame. This result will be shown later to be in serious disagreement with numerical simulations of the Navier–Stokes equations.

Equation (9) has an equilibrium solution (in the limit as $t^* \to \infty$) which is of the form

$$\left(\frac{SK}{\epsilon}\right)_\infty = \left(\frac{\alpha}{C_\mu}\right)^{\frac{1}{2}}, \tag{13}$$

where $\alpha \equiv (C_{\epsilon 2}-1)/(C_{\epsilon 1}-1)$. Hence, the long-time solutions (i.e. when $t^* \gg 1$) for K^* and ϵ^* behave as

$$K^* \sim \exp\left[\left(\frac{C_\mu}{\alpha}\right)^{\frac{1}{2}}(\alpha-1)\,t^*\right], \tag{14}$$

$$\epsilon^* \sim \exp\left[\left(\frac{C_\mu}{\alpha}\right)^{\frac{1}{2}}(\alpha-1)\,t^*\right], \tag{15}$$

which are obtained by substituting (13) into (11) and (12). Thus the K–ϵ model predicts that there is an exponential growth of K and ϵ in time for homogeneous

turbulent shear flow; a structural equilibrium is reached in terms of the dimensionless ratio SK/ϵ that is completely independent of initial conditions. It is encouraging to note that this physical picture is consistent with direct numerical simulations of the Navier–Stokes equations (see Rogallo 1981) and physical experiments (see Tavoularis & Corrsin 1981) for turbulent shear flow in an inertial framing. However, as we shall soon see, it is qualitatively incorrect for a wide range of rotation rates that lie outside the range $0 \leqslant \Omega/S \leqslant 0.5$.

Speziale (1987) recently proposed a nonlinear K–ϵ model which, for turbulent channel and duct flows, was shown to yield improved predictions for the normal Reynolds stress anisotropies. The Reynolds stress tensor for this nonlinear K–ϵ model generalized for rotating flows is as follows (see Speziale 1989):

$$\tau_{ij} = -\tfrac{2}{3} K \delta_{ij} + 2 C_\mu \frac{K^2}{\epsilon} \bar{S}_{ij} - 4 C_\mu^2 C_D \frac{K^3}{\epsilon^2} (\mathring{\bar{S}}_{ij} + \bar{S}_{ik} \bar{S}_{kj} - \tfrac{1}{3} \bar{S}_{mn} \bar{S}_{mn} \delta_{ij} + 2 \bar{W}_{ik} \bar{S}_{kj} + 2 \bar{W}_{jk} \bar{S}_{ki}),$$

$$(16)$$

where

$$\mathring{\bar{S}}_{ij} \equiv \frac{\partial \bar{S}_{ij}}{\partial t} + \bar{v} \cdot \nabla \bar{S}_{ij} - \bar{\omega}_{ik} \bar{S}_{kj} - \bar{\omega}_{jk} \bar{S}_{ki}, \tag{17}$$

$$\bar{S}_{ij} \equiv \frac{1}{2} \left(\frac{\partial \bar{v}_i}{\partial x_j} + \frac{\partial \bar{v}_j}{\partial x_i} \right), \quad \bar{\omega}_{ij} \equiv \frac{1}{2} \left(\frac{\partial \bar{v}_i}{\partial x_j} - \frac{\partial \bar{v}_j}{\partial x_i} \right), \tag{18}$$

$$\bar{W}_{ij} \equiv \bar{\omega}_{ij} + \epsilon_{mji} \Omega_m \tag{19}$$

are, respectively, the frame-indifferent Jaumann derivative of $\bar{S}$, the mean rate of strain tensor $\bar{S}$, the mean vorticity tensor $\bar{\omega}$, and the intrinsic mean vorticity tensor $\bar{W}$ (i.e. the mean vorticity tensor relative to an inertial framing). It is clear that the traditional K–ϵ model is extracted in the limit as $C_D \to 0$ (C_D was evaluated to be 1.68 by correlating with experimental data for turbulent channel flow; see Speziale 1987). Equation (16) must be solved in conjunction with modelled transport equations for the turbulent kinetic energy and dissipation rate. The same transport equations for K and ϵ as developed for the traditional K–ϵ model (see (2) and (3)) have been used. Consequently, for homogeneous turbulent shear flow in a rotating frame, it can be shown that

$$a_{11} = C_D C_\mu^2 \left(\frac{SK}{\epsilon} \right)^2 \left[\frac{7}{3} - 8 \left(\frac{\Omega}{S} \right) \right], \quad a_{12} = -C_\mu \frac{SK}{\epsilon}, \tag{20}$$

$$a_{22} = C_D C_\mu^2 \left(\frac{SK}{\epsilon} \right)^2 \left[-\frac{5}{8} + 8 \left(\frac{\Omega}{S} \right) \right], \quad a_{33} = -\tfrac{2}{3} C_D C_\mu^2 \left(\frac{SK}{\epsilon} \right)^2 \tag{21}$$

for the nonlinear K–ϵ model. Since a_{12} is of the same form for both the nonlinear and linear K–ϵ model, it follows that the transport equations for K and ϵ corresponding to (20) and (21) are the same as their linear counterparts. More specifically, (20) and (21) are solved along with the transport equations (5) and (6) which yield the same results for K and ϵ as obtained from the traditional K–ϵ model (most notably, this means that the equilibrium value of $(SK/\epsilon)_\infty$ is the same as given in (13) for the traditional K–ϵ model). Hence, the nonlinear K–ϵ model of Speziale (1987, 1989) only gives rise to differences in the normal components of the anisotropy tensor. Later, it will be shown how these differences constitute a substantial improvement over the traditional K–ϵ model.

Perhaps the most popular second-order closure model currently used is that of Launder, Reece & Rodi (1975). In the simplified form of this model† (which will

† This simplified form of the LRR model is now referred to as the Basic Model by Launder and his coworkers.

hereinafter be referred to as the LRR model), the Reynolds stress tensor is a solution of the transport equation

$$\dot{\tau}_{ij} = (C_2 - 1)\left(\tau_{ik}\frac{\partial \bar{v}_j}{\partial x_k} + \tau_{jk}\frac{\partial \bar{v}_i}{\partial x_k}\right) + (C_2 - 2)\,(\tau_{ik}\,\epsilon_{mkj}\,\Omega_m + \tau_{jk}\,\epsilon_{mki}\,\Omega_m)$$

$$- C_1\frac{\epsilon}{K}(\tau_{ij} + \tfrac{2}{3}K\delta_{ij}) - \tfrac{2}{3}C_2\,\tau_{kl}\frac{\partial \bar{v}_k}{\partial x_l}\delta_{ij} + \tfrac{2}{3}\epsilon\delta_{ij}, \quad (22)$$

which has been simplified to a form valid for any rotating homogeneous turbulence. In (22), C_1 and C_2 are empirical constants usually taken to be 1.8 and 0.6, respectively. This Reynolds stress transport model is solved in conjunction with the modelled dissipation rate equation (3) where $C_{\epsilon 1} = 1.45$ and $C_{\epsilon 2} = 1.90$. For the problem of homogeneous turbulent shear flow in a rotating frame, the LRR model yields the following system of coupled nonlinear ordinary differential equations:

$$\dot{K} = \tau_{12}S - \epsilon, \tag{23}$$

$$\dot{\epsilon} = C_{\epsilon 1}\frac{\epsilon}{K}\tau_{12}S - C_{\epsilon 2}\frac{\epsilon^2}{K}, \tag{24}$$

$$\dot{\tau}_{12} = \tau_{22}S + (C_2 - 2)[\Omega\tau_{11} + \tau_{22}(S - \Omega)] - C_1\frac{\epsilon}{K}\tau_{12}, \tag{25}$$

$$\dot{\tau}_{11} = 2\tau_{12}S + 2(C_2 - 2)(S - \Omega)\tau_{12} - C_1\frac{\epsilon}{K}(\tau_{11} + \tfrac{2}{3}K) - \tfrac{2}{3}C_2\tau_{12}S + \tfrac{2}{3}\epsilon, \tag{26}$$

$$\dot{\tau}_{22} = 2\Omega(C_2 - 2)\tau_{12} - C_1\frac{\epsilon}{K}(\tau_{22} + \tfrac{2}{3}K) - \tfrac{2}{3}C_2\tau_{12}S + \tfrac{2}{3}\epsilon. \tag{27}$$

Since
$$\tau_{33} = -(\tau_{11} + \tau_{22} + 2K) \tag{28}$$

it is not necessary to solve the transport equation for τ_{33}. The system of equations (23)–(27) can be non-dimensionalized and recast into an alternative system of equations for ϵ/SK, a_{11}, a_{12}, a_{22} and K^*, which are as follows:

$$\frac{\mathrm{d}}{\mathrm{d}t^*}\left(\frac{\epsilon}{SK}\right) = (1 - C_{\epsilon 1})\left(\frac{\epsilon}{SK}\right)a_{12} + (1 - C_{\epsilon 2})\left(\frac{\epsilon}{SK}\right)^2, \tag{29}$$

$$\frac{\mathrm{d}K^*}{\mathrm{d}t^*} = -\left(a_{12} + \frac{\epsilon}{SK}\right)K^*, \tag{30}$$

$$\frac{\mathrm{d}a_{12}}{\mathrm{d}t^*} = (C_2 - 1)(a_{22} + \tfrac{2}{3}) + (C_2 - 2)\left[\frac{\Omega}{S}(a_{11} - a_{22})\right] - (C_1 - 1)\left(\frac{\epsilon}{SK}\right)a_{12} + a_{12}^2, \tag{31}$$

$$\frac{\mathrm{d}a_{11}}{\mathrm{d}t^*} = 2\left[(2 - C_2)\frac{\Omega}{S} + \tfrac{2}{3}(C_2 - 1)\right]a_{12} + (1 - C_1)\left(\frac{\epsilon}{SK}\right)a_{11} + a_{12}a_{11}, \tag{32}$$

$$\frac{\mathrm{d}a_{22}}{\mathrm{d}t^*} = 2\left[(C_2 - 2)\frac{\Omega}{S} - \tfrac{1}{3}(C_2 - 1)\right]a_{12} + (1 - C_1)\left(\frac{\epsilon}{SK}\right)a_{22} + a_{12}a_{22}, \tag{33}$$

where again $t^* = St$ is the dimensionless time. These nonlinear ordinary differential equations are solved subject to the initial conditions

$$\frac{\epsilon}{SK} = \frac{\epsilon_0}{SK_0}, \quad a_{11} = 0, \quad a_{12} = 0, \quad a_{22} = 0 \tag{34}$$

at time $t^* = 0$, which correspond to a state of isotropy (the same conditions that are

usually taken in physical and numerical experiments). It should be noted that a_{33} and ϵ^* can be obtained from the computed variables as follows:

$$\epsilon^* = \frac{\epsilon}{SK}\left(\frac{SK_0}{\epsilon_0}\right)K^*, \tag{35}$$

$$a_{33} = -(a_{11} + a_{22}). \tag{36}$$

It is also interesting to note that the shear rate only enters into the solution of the problem through the initial condition SK_0/ϵ_0. Hence, there can be equilibrium solutions that only depend on a single parameter – the ratio of the rotation rate to the shear rate Ω/S. Such equilibrium states are of the form

$$\frac{\epsilon}{SK} = \left(\frac{\epsilon}{SK}\right)_\infty, \quad a_{11} = (a_{11})_\infty, \quad a_{12} = (a_{12})_\infty, \quad a_{22} = (a_{22})_\infty \tag{37}$$

in the limit as $t^* \to \infty$. In dynamical systems terms, (37) constitute the fixed points in the four-dimensional phase space $(\epsilon/SK, a_{11}, a_{12}, a_{22})$ of equations (29), (31), (32) and (33). Mathematically, these fixed points are determined by setting the time derivatives of ϵ/SK, a_{11}, a_{12} and a_{22} to zero. This yields the nonlinear system of algebraic equations

$$\frac{\epsilon}{SK}\left[(1-C_{\epsilon 1})a_{12} + (1-C_{\epsilon 2})\left(\frac{\epsilon}{SK}\right)\right] = 0, \tag{38}$$

$$(C_2-1)(a_{22}+\tfrac{2}{3}) + (C_2-2)\left[\frac{\Omega}{S}(a_{11}-a_{22})\right] - (C_1-1)\frac{\epsilon}{SK}a_{12} + a_{12}^2 = 0, \tag{39}$$

$$2\left[(2-C_2)\frac{\Omega}{S} + \frac{2}{3}(C_2-1)\right]a_{12} + (1-C_1)\left(\frac{\epsilon}{SK}\right)a_{11} + a_{12}a_{11} = 0, \tag{40}$$

$$2\left[(C_2-2)\frac{\Omega}{S} - \frac{1}{3}(C_2-1)\right]a_{12} + (1-C_1)\left(\frac{\epsilon}{SK}\right)a_{22} + a_{12}a_{22} = 0, \tag{41}$$

whose solutions will be examined in the next section.

The Rotta–Kolmogorov model (cf. Mellor & Herring 1973) will now be considered. Since this model been applied to a variety of geophysical fluid dynamics problems involving system rotations (cf. Mellor & Yamada 1974), its performance in predicting homogeneous turbulent shear flow in a rotating frame is of interest. For a general homogeneous turbulence in a rotating frame, the Rotta–Kolmogorov model (which will hereinafter be referred to as the RK model) takes the form

$$\dot{\tau}_{ij} = -\tau_{im}\left(\frac{\partial \bar{v}_j}{\partial x_m} + 2\epsilon_{nmj}\Omega_m\right) - \tau_{jm}\left(\frac{\partial \bar{v}_i}{\partial x_m} + 2\epsilon_{nmi}\Omega_n\right)$$

$$-\frac{\sqrt{2}K^{\frac{1}{2}}}{3A_1 l}(\tau_{ij} + \tfrac{2}{3}K\delta_{ij}) - 2C_1 K\left(\frac{\partial \bar{v}_i}{\partial x_j} + \frac{\partial \bar{v}_j}{\partial x_i}\right) + \frac{4}{3}\frac{\sqrt{2}K^{\frac{3}{2}}}{B_1 l}\delta_{ij}, \tag{42}$$

$$\dot{Kl} = \tfrac{1}{2}El\tau_{ij}\frac{\partial \bar{v}_i}{\partial x_j} - \frac{\sqrt{2}}{B_1}K^{\frac{3}{2}}, \tag{43}$$

where l is the lengthscale of turbulence, and A_1, B_1, C_1 and E are empirical constants which are taken to be 0.78, 15.0, 0.056 and 1.4, respectively. For homogeneous

turbulent shear flow in a rotating frame, (42) and (43) yield the following system of nonlinear ordinary differential equations:

$$\dot{K} = \tau_{12} S - \frac{2\sqrt{2}}{B_1} \frac{K^{\frac{3}{2}}}{l},$$ (44)

$$\dot{Kl} = \tfrac{1}{2} E l \tau_{12} S - \frac{\sqrt{2}}{B_1} K^{\frac{3}{2}},$$ (45)

$$\dot{\tau}_{12} = -\frac{\sqrt{2}}{3A_1} \frac{K^{\frac{1}{2}}}{l} \tau_{12} - 2C_1 KS - \tau_{22} S + 2\Omega(\tau_{22} - \tau_{11}),$$ (46)

$$\dot{\tau}_{11} = -\frac{\sqrt{2}}{3A_1} \frac{K^{\frac{1}{2}}}{l} (\tau_{11} + \tfrac{2}{3}K) - 2\tau_{12}(S - 2\Omega) + \frac{4\sqrt{2}}{3B_1} \frac{K^{\frac{3}{2}}}{l},$$ (47)

$$\dot{\tau}_{22} = -\frac{\sqrt{2}}{3A_1} \frac{K^{\frac{1}{2}}}{l} (\tau_{22} + \tfrac{2}{3}K) - 4\tau_{12}\Omega + \frac{4\sqrt{2}}{3B_1} \frac{K^{\frac{3}{2}}}{l}.$$ (48)

However, the decay of turbulent kinetic energy is governed by the equation

$$\dot{K} = \tau_{12} S - \epsilon,$$ (49)

which is a rigorous consequence of the Navier–Stokes equations for the homogeneous turbulent shear flow under consideration. A simple comparison of (44) and (49) yields

$$l = \frac{2\sqrt{2}}{B_1} \frac{K^{\frac{3}{2}}}{\epsilon}$$ (50)

for the RK model. Hence, as with the LRR model, the system of equations (44)–(48) can be non-dimensionalized and recast into an equivalent set of equations for SK/ϵ, a_{11}, a_{12} and a_{22} as follows:

$$\frac{d}{dt^*}\left(\frac{\epsilon}{SK}\right) = (\tfrac{1}{2}E - \tfrac{3}{2})\frac{\epsilon}{SK} a_{12} - \left(\frac{\epsilon}{SK}\right)^2,$$ (51)

$$\frac{da_{12}}{dt^*} = 2(C_1 - \tfrac{1}{3}) - a_{22} + \left(1 - \frac{B_1}{6A_1}\right)\frac{\epsilon}{SK} a_{12} - 2\frac{\Omega}{S}(a_{11} - a_{22}) + a_{12}^2,$$ (52)

$$\frac{da_{11}}{dt^*} = 4\left(\frac{\Omega}{S} - \frac{1}{3}\right)a_{12} + \left(1 - \frac{B_1}{6A_1}\right)\frac{\epsilon}{SK} a_{11} + a_{12}a_{11},$$ (53)

$$\frac{da_{22}}{dt^*} = -2\left(2\frac{\Omega}{S} - \frac{1}{3}\right)a_{12} + \left(1 - \frac{B_1}{6A_1}\right)\frac{\epsilon}{SK} a_{22} + a_{12}a_{22}.$$ (54)

This system of nonlinear ordinary differential equations is solved subject to the initial conditions (34) which correspond to an isotropic turbulence. As with the LRR model, K^*, ϵ^* and a_{33} are obtained from the computed variables using (30), (35) and (36) which are model independent. The equilibrium states corresponding to the RK model are obtained by setting the time derivatives to zero in (51)–(54) which yields the nonlinear algebraic equations

$$(\tfrac{1}{2}E - \tfrac{3}{2})\frac{\epsilon}{SK} a_{12} - \left(\frac{\epsilon}{SK}\right)^2 = 0,$$ (55)

$$2(C_1 - \tfrac{1}{3}) - a_{22} + \left(1 - \frac{B_1}{6A_1}\right)\frac{\epsilon}{SK} a_{12} - 2\frac{\Omega}{S}(a_{11} - a_{22}) + a_{12}^2 = 0,$$ (56)

$$4\left(\frac{\Omega}{S}-\frac{1}{3}\right)a_{12}+\left(1-\frac{B_1}{6A_1}\right)\frac{\epsilon}{SK}a_{11}+a_{12}a_{11}=0, \tag{57}$$

$$-2\left(2\frac{\Omega}{S}-\frac{1}{3}\right)a_{12}+\left(1-\frac{B_1}{6A_1}\right)\frac{\epsilon}{SK}a_{22}+a_{12}a_{22}=0. \tag{58}$$

The equations of motion for the RK model are of the same general form as those for the LRR model (only the values of the coefficients are altered). Hence, both second-order closure models have the same topological properties. For example, both models have exponential long-time growth behaviour, i.e.

$$K^* \sim \exp\left\{\left|(a_{12})_\infty+\left(\frac{\epsilon}{SK}\right)_\infty\right|t^*\right\}, \tag{59}$$

$$\epsilon^* \sim \exp\left\{\left|(a_{12})_\infty+\left(\frac{\epsilon}{SK}\right)_\infty\right|t^*\right\} \tag{60}$$

for $t^* \gg 1$ and $(\epsilon/SK)_\infty > 0$† (it should be noted that Tavoularis (1985) predicted such an exponential growth for the spatially evolving version of homogeneous turbulent shear flow obtained by a Galilean transformation). Furthermore, the bifurcation diagrams for these models are qualitatively similar.

Finally, we shall consider the Shih–Lumley model (Shih & Lumley 1985; and T. H. Shih 1988, private communication) which constitutes one of the newer second-order closure models that has received considerable attention during the past few years. This model (hereinafter referred to as the SL model) is noteworthy for its satisfaction of realizability (Lumley 1978) and for its more elaborate treatment of the pressure–strain correlation. For any homogeneous turbulence in a rotating frame, the SL model takes the form

$$\dot{\tau}_{ij} = -\tau_{im}\left(\frac{\partial \bar{v}_j}{\partial x_m}-2\epsilon_{njm}\Omega_n\right)-\tau_{jm}\left(\frac{\partial \bar{v}_i}{\partial x_m}-2\epsilon_{nim}\Omega_n\right)-4(\tfrac{1}{5}+2\alpha_5)K\bar{S}_{ij}$$

$$+\tfrac{2}{3}(1-\alpha_5)\left[\tau_{ik}\left(\frac{\partial \bar{v}_j}{\partial x_k}+\epsilon_{mkj}\Omega_m\right)+\tau_{jk}\left(\frac{\partial \bar{v}_i}{\partial x_k}+\epsilon_{mki}\Omega_m\right)-\tfrac{2}{3}\tau_{kl}\bar{S}_{kl}\delta_{ij}\right]$$

$$-(\tfrac{2}{3}+\tfrac{16}{3}\alpha_5)\left[\tau_{ik}\left(\frac{\partial \bar{v}_k}{\partial x_j}+\epsilon_{mjk}\Omega_m\right)+\tau_{jk}\left(\frac{\partial \bar{v}_k}{\partial x_i}+\epsilon_{mik}\Omega_m\right)-\tfrac{2}{3}\tau_{kl}\bar{S}_{kl}\delta_{ij}\right]$$

$$-\tfrac{6}{5}\tau_{kl}\bar{S}_{kl}b_{ij}-\tfrac{2}{15}[2\tau_{ik}(\bar{\omega}_{jk}+\epsilon_{mkj}\Omega_m)+2\tau_{jk}(\bar{\omega}_{ik}+\epsilon_{mki}\Omega_m)]$$

$$-\frac{1}{5K}\left\{\left[\tau_{ik}\left(\frac{\partial \bar{v}_j}{\partial x_l}+\epsilon_{mlj}\Omega_m\right)+\tau_{jk}\left(\frac{\partial \bar{v}_i}{\partial x_l}+\epsilon_{mli}\Omega_m\right)\right]\tau_{kl}-2\tau_{il}\tau_{jm}\bar{S}_{lm}\right\}$$

$$+\beta\epsilon b_{ij}+\tfrac{2}{3}\epsilon\delta_{ij}, \tag{61}$$

where

$$\alpha_5 = -\tfrac{1}{10}(1+0.8F^{\frac{1}{2}}), \quad F = 1+27III+9II, \tag{62}$$

$$II = -\tfrac{1}{2}b_{ij}b_{ij}, \quad III = \tfrac{1}{3}b_{ij}b_{jk}b_{ki}, \quad b_{ij} = \tfrac{1}{2}a_{ij}, \tag{63}$$

$$\beta = 2+\tfrac{1}{6}F\{80.1\ln[1+62.4(-II+2.3III)]\}. \tag{64}$$

† For $(\epsilon/SK)_\infty = 0$, it will be demonstrated later that K and ϵ can either grow or decay with time.

The dissipation rate ϵ is obtained from a modelled transport equation of the form

$$\dot{\epsilon} = C_{\epsilon1}^* \frac{\epsilon}{K} \tau_{ij} \frac{\partial \bar{v}_i}{\partial x_j} - C_{\epsilon2}^* \frac{\epsilon^2}{K}, \tag{65}$$

where
$$C_{\epsilon1}^* = 1.44, \quad C_{\epsilon2}^* = \tfrac{7}{5} + 0.49[1 - 0.33 \ln(1 - 55II)] \tag{66}$$

for high-Reynolds-number flows. The SL model equations for homogeneous shear flow in a rotating frame are obtained by substituting (1) and (18) into (61) and (65) while making use of the fact that $\Omega_i = (0, 0, \Omega)$. These equations take the form

$$\dot{K} = \tau_{12} S - \epsilon, \tag{67}$$

$$\dot{\epsilon} = c_{\epsilon1}^* \frac{\epsilon}{K} \tau_{12} S - c_{\epsilon2}^* \frac{\epsilon^2}{K}, \tag{68}$$

$$\dot{\tau}_{11} = -2(S - 2\Omega)\tau_{12} + \beta\epsilon b_{11} + \tfrac{2}{3}\epsilon + (\tfrac{4}{3} + \tfrac{14}{3}\alpha_5)(\tfrac{2}{3}S - 2\Omega)\tau_{12}$$
$$+ \tfrac{4}{9}(1 - \alpha_5)\tau_{12}S - \tfrac{6}{5}b_{11}\tau_{12}S - \tfrac{4}{15}(S - 2\Omega)\tau_{12} - \frac{2}{5K}[(S - \Omega)(\tau_{11}\tau_{12} + \tau_{12}\tau_{22})$$
$$- \tau_{11}\tau_{12}S], \quad (69)$$

$$\dot{\tau}_{12} = -2\Omega\tau_{11} - (S - 2\Omega)\tau_{22} + \beta\epsilon b_{12} - 2(\tfrac{1}{5} + 2\alpha_5)KS$$
$$- (\tfrac{4}{3} + \tfrac{14}{3}\alpha_5)[\tau_{11}S - (\tau_{11} - \tau_{22})\Omega] + \tfrac{2}{3}(1 - \alpha_5)(\tau_{11} + \tau_{22})S$$
$$- \tfrac{6}{5}b_{12}\tau_{12}S + \tfrac{2}{15}(S - 2\Omega)(\tau_{11} - \tau_{22}) - \frac{1}{5K}[\tau_{22}^2(S - \Omega) + \tau_{11}^2\Omega - \tau_{11}\tau_{22}S], \quad (70)$$

$$\dot{\tau}_{22} = -4\Omega\tau_{12} + \beta\epsilon b_{22} + \tfrac{2}{3}\epsilon - (\tfrac{4}{3} + \tfrac{14}{3}\alpha_5)(\tfrac{2}{3}S - 2\Omega)\tau_{12}$$
$$- \tfrac{2}{3}(\tfrac{2}{3} + \tfrac{16}{3}\alpha_5)\tau_{12}S - \tfrac{6}{5}b_{22}\tau_{12}S + \tfrac{4}{15}(S - 2\Omega)\tau_{12} - \frac{2}{5K}[\Omega\tau_{11}\tau_{12} - (S - \Omega)\tau_{12}\tau_{22}]. \quad (71)$$

We shall not bother to convert the system (67)–(71) into the variables $(b_{11}, b_{12}, b_{22}, \epsilon/SK)$ since, owing to the highly nonlinear nature of these equations, a closed-form analysis of its equilibrium states is not possible. The equilibrium states of the SL model will be obtained solely from a numerical integration of (67)–(71). A comparison of the results predicted by each of the models with physical and numerical experiments will be made in the next section.

3. Comparison of the models

First, we shall present computed results for the time evolution of the turbulent kinetic energy and dissipation rate predicted by the various models. It should be noted that both the traditional and nonlinear K–ϵ models yield the same results for the time evolution of K^* and ϵ^* (the differences between the two models are in their predictions for the anisotropy tensor). Computations were conducted for a variety of values of Ω/S using a Runge–Kutta–Fehlburg numerical integration scheme. In figures 2 and 3, the time evolution of the turbulent kinetic energy and dissipation rate are shown for $\Omega/S = 0$ and an initial condition of $\epsilon_0/SK_0 = 0.296$ (picked to agree with the large-eddy simulations of Bardina, Ferziger & Reynolds 1983). All of the models except the SL model are in the range of the results obtained from the large-eddy simulations. Three observations are noteworthy: (a) there is not a substantial difference between the quality of the predictions of the K–ϵ model and the
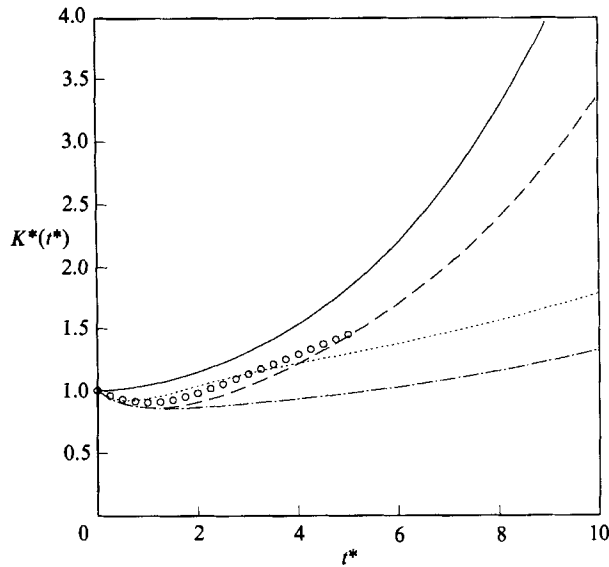
FIGURE 2. Time evolution of the turbulent kinetic energy for homogeneous shear flow: $\Omega/S = 0$, $\epsilon_0/SK_0 = 0.296$. ———, K–ϵ model; ....., Rotta–Kolmogorov (RK) model; ––, Launder *et al.* (LRR) model; –··–, Shih–Lumley (SL) model; ○, large-eddy simulation of Bardina *et al.* (1983).
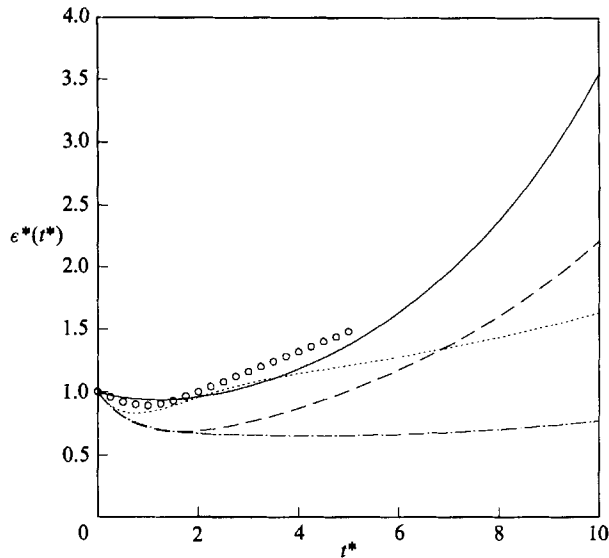

FIGURE 3. Time evolution of the turbulent dissipation rate for homogeneous shear flow: $\Omega/S = 0$, $\epsilon_0/SK_0 = 0.296$. Symbols as in figure 2.

LRR model for $t^* < 6$; (b) the RK model is well within the range of the large-eddy simulations but it gives rise to noticeable points of inflection that appear to be unphysical; and (c) the SL model is much less energetic than the other models as well as the large-eddy simulations.

Direct comparisons with the experiments of Champagne *et al.* (1970) are somewhat tenuous owing to the uncertainty as to what the initial dissipation was in that study. Mild to moderate changes in the initial dissipation (reflected in the initial condition
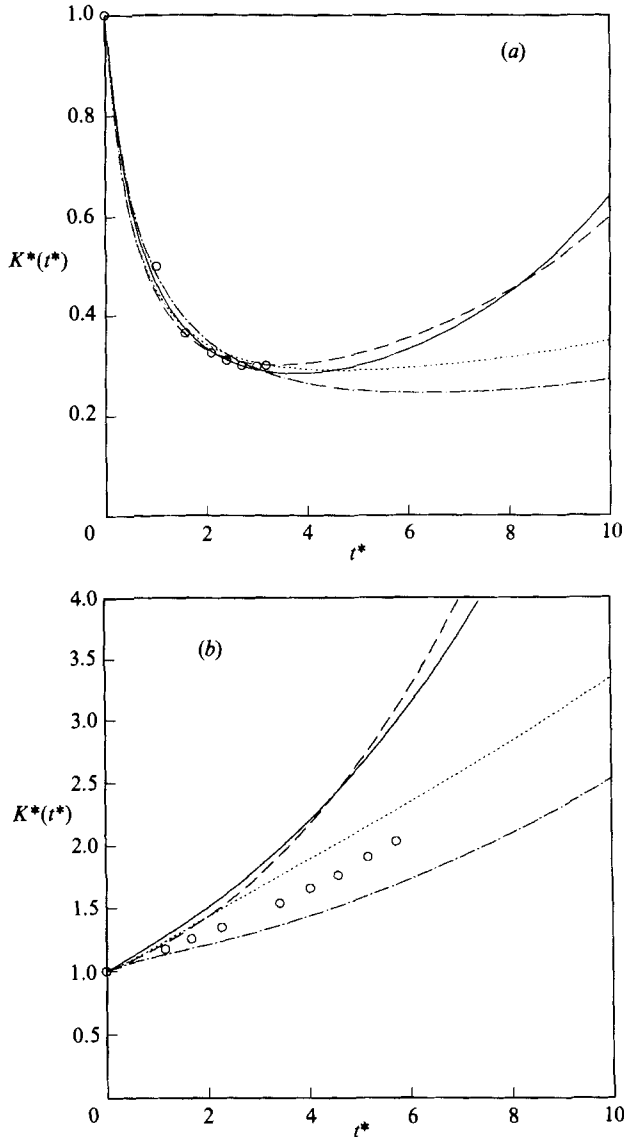
FIGURE 4. Time evolution of the turbulent kinetic energy for homogeneous shear flow: comparison of the models with physical experiments. (a) Champagne *et al.* (1970) experiment; (b) Tavoularis & Corrsin (1981) experiment. Symbols as in figure 2.

ϵ_0/SK_0) can yield considerably different results for the time evolution of the turbulent kinetic energy and dissipation rate. In figure 4(a), it is shown that all of the models can be made to fit the Champagne *et al.* (1970) data for different initial conditions on ϵ_0/SK_0 which range from 1.2 to 1.5† – values that are within the range of what can be extrapolated from the Champagne *et al.* data. For $t^* > 8$, the models yield considerably different results for the turbulent kinetic energy despite the fact that they match the Champagne *et al.* data for $t^* < 4$. Consequently, the Champagne *et al.* experiment constitutes a rather weak test for turbulence models. The

† ϵ_0/SK_0 is 1.2 for the SL model, 1.3 for the K-ϵ model, 1.4 for the LRR model and 1.5 for the RK model.
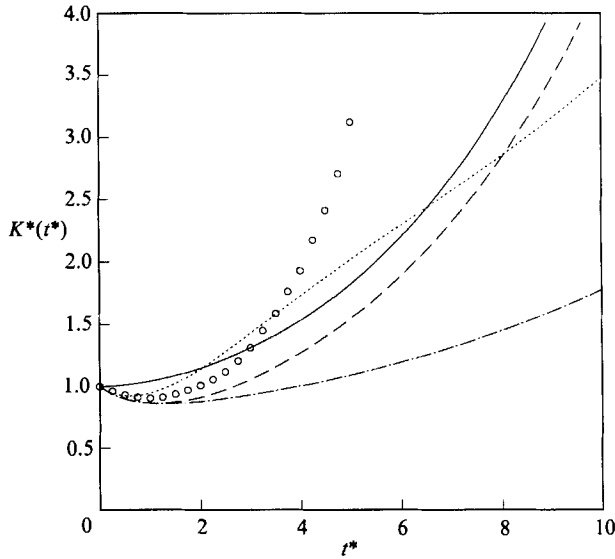
FIGURE 5. Time evolution of the turbulent kinetic energy for rotating homogeneous shear flow: $\Omega/S = 0.25$, $\epsilon_0/SK_0 = 0.296$. Symbols as in figure 2.
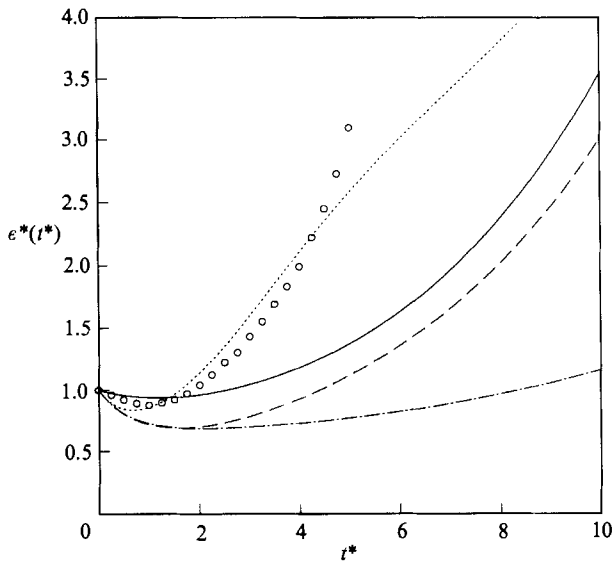

FIGURE 6. Time evolution of the turbulent dissipation rate for rotating homogeneous shear flow: $\Omega/S = 0.25$, $\epsilon_0/SK_0 = 0.296$. Symbols as in figure 2.

experimental data of Tavoularis & Corrsin (1981) represent a more stringent test since the shear rate S is larger than that for the Champagne *et al.* experiment and since the initial conditions are specified more completely. In figure 4(*b*), the time evolution of the turbulent kinetic energy predicted by the various models is compared with the experimental data of Tavoularis & Corrsin (1981). It should be noted that $t^* = 0$ corresponds to $St \approx 6.75$ in the Tavoularis–Corrsin experiment for which b_{ij} and SK/ϵ are provided therein (hence, the uncertainty in the initial conditions is overcome). It is clear from figure 4(*b*) that the RK model and the SL
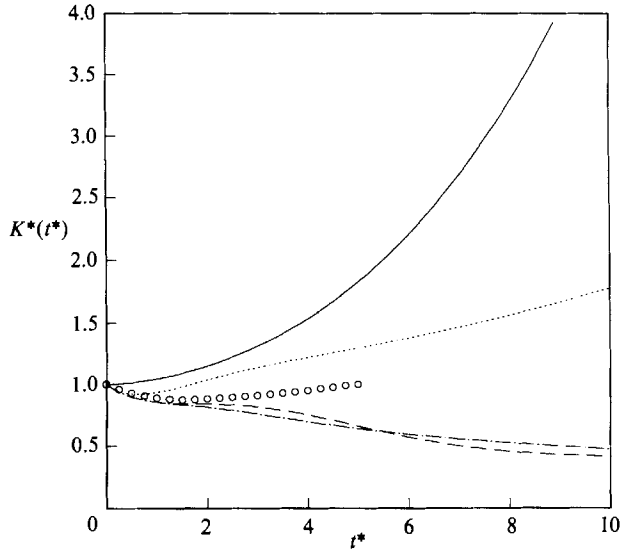
FIGURE 7. Time evolution of the turbulent kinetic energy for rotating homogeneous shear flow: $\Omega/S = 0.5$, $\epsilon_0/SK_0 = 0.296$. Symbols as in figure 2.
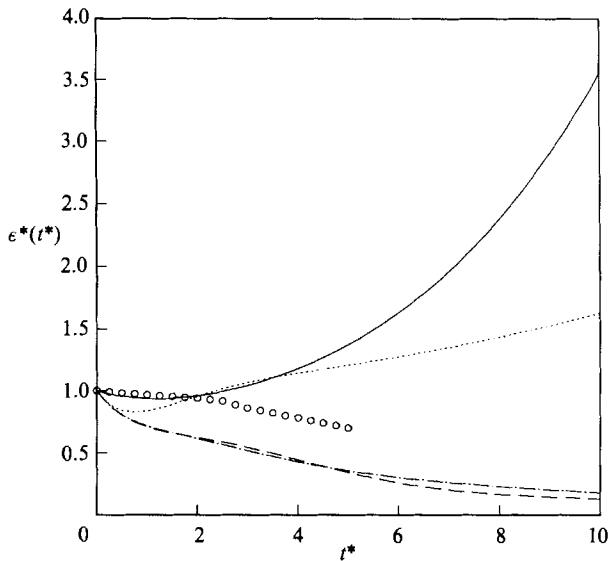
FIGURE 8. Time evolution of the turbulent dissipation rate for rotating homogeneous shear flow: $\Omega/S = 0.5$, $\epsilon_0/SK_0 = 0.296$. Symbols as in figure 2.

model do a reasonably good job in predicting the time evolution of the turbulent kinetic energy. However, the K–ϵ model and the LRR model appear to be somewhat too energetic.

Although the models considered in this study do reasonably well for pure shear, it will now be shown that the quality of the predictions degrades considerably with the imposition of a system rotation. In figures 5 and 6, the time evolution of the turbulent kinetic energy and dissipation rate are shown for $\Omega/S = 0.25$ and the same initial condition of $\epsilon_0/SK_0 = 0.296$. From figures 5 and 6, it is clear that all of the

	Equilibrium values	Linear K–ϵ model	Nonlinear K–ϵ model	Experiments	Large-eddy simulations
$\Omega/S = 0$	a_{11}	0	0.431	0.403	0.61
	a_{22}	0	−0.308	−0.295	−0.53
	a_{12}	−0.332	−0.332	−0.284	−0.29
	SK/ϵ	6.03	6.03	6.08	—
$\Omega/S = 0.25$	a_{11}	0	0.062	—	0.12
	a_{22}	0	0.062	—	0.09
	a_{12}	−0.332	−0.332	—	−0.70
	SK/ϵ	6.03	6.03	—	—
$\Omega/S = 0.5$	a_{11}	0	−0.308	—	−0.53
	a_{22}	0	0.431	—	0.50
	a_{12}	−0.332	−0.332	—	−0.20
	SK/ϵ	6.03	6.03	—	—

TABLE 1. Equilibrium results for homogeneous turbulent shear flow in a rotating frame: comparison of the predictions of the K–ϵ model with the large-eddy simulations of Bardina *et al.* (1983) and the experiments of Tavoularis & Corrsin (1981).

models substantially underpredict the turbulent kinetic energy and dissipation rate in comparison to the results of the large-eddy simulation of Bardina *et al.* (1983). This discrepancy appears to be serious since the rather dramatic increase in turbulence activity indicated by the large-eddy simulations in figure 5 has been confirmed independently by linear spectral models (see figure 3 in Bertoglio 1982). In addition, one would expect, on physical grounds, the case of $\Omega/S = 0.25$ to be substantially more energetic than the case of $\Omega/S = 0$. When third-order moments are neglected in the Reynolds stress transport equations, the equations associated with the $\Omega/S = 0.25$ case are identical to those for plane strain and it is well known that plane strain is considerably more energetic than plane shear in homogeneous turbulence. Unfortunately, there are no published experiments with which the models can be compared.

The time evolution of the turbulent kinetic energy and dissipation rate for $\Omega/S = 0.5$ and an initial condition of $\epsilon_0/SK_0 = 0.296$ is shown in figures 7 and 8. It appears that the RK model yields results that are in the best agreement with the large-eddy simulations. The LRR model and the SL model yield qualitatively different predictions for this case in comparison to the RK model (the former models predict that the turbulence decays whereas the latter model predicts a weak exponential growth). This considerable disparity in the predictions of the models arises from the way in which the rapid pressure–strain is modelled. The LRR and SL modelling of this term destroys similitude with respect to the Richardson number – a similarity property which the RK model has (see Speziale & Mac Giolla Mhuiris 1989). The Richardson number

$$Ri = \frac{-2\Omega(S-2\Omega)}{S^2} \qquad (72)$$

is zero for the two cases of $\Omega/S = 0$ and $\Omega/S = 0.5$. Here, the RK model yields the same results for both cases; the LRR model and SL model yield qualitatively different results for the two cases; and large-eddy simulations indicate that the two cases are quantitatively distinct but qualitatively similar. It should be noted that the prediction of a decaying turbulence for sufficiently large values of $\Omega/S > 0.5$ is physically correct and will be discussed later. However, large-eddy simulations and

alternative theoretical analyses indicate that the flow should be unstable for at least the range $0 \leqslant \Omega/S \leqslant 0.5$.

The equilibrium states associated with the K–ϵ model for rotating shear flow were derived earlier in (8), (13), (20) and (21). In table 1, the specific numerical values of the equilibrium anisotropy tensor a_{ij} and shear parameter SK/ϵ are given as a function of Ω/S for both the linear and nonlinear K–ϵ models. It should be pointed out that these results were computed using the value of $C_\mu = 0.055$ which was recommended by Rodi (1972) for ratios of production to dissipation P/ϵ of the order of 2 or greater (for the problem at hand, $P/\epsilon = 2$). The traditional value of $C_\mu = 0.09$ was used for the time evolution computations shown in figures 2 and 3 since it rigorously applies for $P/\epsilon = 1$ (the mean between the initial value of $P/\epsilon = 0$ and the equilibrium value of $P/\epsilon = 2$) and thus constitutes a reasonable average for C_μ that is used in most engineering calculations where there is a temporally or spatially varying turbulence structure. It is clear that the equilibrium values shown in table 1 for the linear K–ϵ model are extremely poor in their prediction of the normal components of the anisotropy tensor. The nonlinear K–ϵ model yields considerably improved predictions for these normal components of the anisotropy tensor (it should be noted that the large-eddy simulations tend to overpredict the anisotropy tensor because the flow was not defiltered). However, both the linear and nonlinear K–ϵ models yield equilibrium values of a_{12} and SK/ϵ which are the same for all values of Ω/S. While these predictions for $(SK/\epsilon)_\infty$ are reasonably good for $\Omega/S = 0$, they can be in serious error for other values of Ω/S. Specifically, for large values of Ω/S, a relaminarization of the flow would be anticipated on physical grounds where the turbulence decays in such a way that $(\epsilon/SK)_\infty = 0$. Such a relaminarization would be expected since, when $\Omega/S > 1$, the Rossby number $(\epsilon/2\Omega K)_\infty < 0.1$. A Taylor–Proudman reorganization of the flow to a two-dimensional state can then occur (see Tritton 1977), and the preponderance of evidence indicates that uniform shear flow is stable to large-amplitude two-dimensional disturbances (see Patera & Orszag 1981). Therefore, any significant trend towards a two-dimensionalization would be accompanied by a relaminarization. Linear spectral models suggest that uniform shear flow is unstable for $Ri \leqslant 0$ (i.e. $0 \leqslant \Omega/S \leqslant 0.5$). Although precise bounds for the stability of uniform shear flow in a rotating framework have not been established, it is generally believed that this flow is stable for Richardson numbers that are somewhat greater than zero (e.g. for $Ri > 0.25$; see Bertoglio 1982). Hence, it is clear that $(SK/\epsilon)_\infty$ must vary considerably with Ω/S, in conflict with results predicted by the K–ϵ model.

The equilibrium states associated with LRR model are solutions of the nonlinear algebraic equations (38)–(41). Non-zero values of $(\epsilon/SK)_\infty$ occur for $-0.0904 < \Omega/S < 0.3761$ where the equilibrium states are given by

$$\left(\frac{\epsilon}{SK}\right)_\infty = \pm \frac{2(2-C_2)}{(1-\alpha-C_1)}\left[\frac{(1-C_2)(C_1+\alpha C_2-1)}{6\alpha(2-C_2)^2} + \left(\frac{1-C_2}{2-C_2}\right)\frac{\Omega}{S} - \left(\frac{\Omega}{S}\right)^2\right]^{\frac{1}{2}}, \qquad (73)$$

$$\left(a_{12}\right)_\infty = -\alpha\left(\frac{\epsilon}{SK}\right)_\infty, \qquad (74)$$

$$\alpha = \frac{C_{\epsilon 2}-1}{C_{\epsilon 1}-1}, \qquad (75)$$

$$(a_{11})_\infty = \frac{2\alpha[(2-C_2)(\Omega/S) - \frac{2}{3}(1-C_2)]}{1-\alpha-C_1}, \tag{76}$$

$$(a_{22})_\infty = \frac{-2\alpha[(2-C_2)(\Omega/S) - \frac{1}{3}(1-C_2)]}{1-\alpha-C_1}, \tag{77}$$

$$(a_{33})_\infty = \frac{\frac{2}{3}\alpha(1-C_2)}{1-\alpha-C_1}. \tag{78}$$

By linear analysis, it can be shown that the upper branch $(\epsilon/SK)_\infty > 0$ is a stable fixed point of the focus type; the lower branch $(\epsilon/SK)_\infty$ is an unstable fixed point of the same type. Of course, realizability requires that $\epsilon/SK > 0$. Thus, it is interesting to note that realizability is satisfied by this model through the presence of the unstable branch $(\epsilon/SK)_\infty = 0$ which is an invariant plane (i.e. solutions that originate in the upper half-plane $(\epsilon/SK_0) > 0$ of the phase space remain there for all times $t > 0$). Hence, realizable initial conditions ensure realizable solutions for all time. Equilibrium solutions for the LRR model where $(\epsilon/SK)_\infty = 0$ and $(a_{12})_\infty = 0$ exist for all Ω/S and are of the form

$$(\epsilon/SK)_\infty = 0, \quad (a_{12})_\infty = 0, \tag{79}$$

$$(a_{11})_\infty = \left[1 - \frac{1-C_2}{2-C_2}\left(\frac{S}{\Omega}\right)\right](a_{22})_\infty - \frac{2}{3}\left(\frac{S}{\Omega}\right)\left(\frac{1-C_2}{2-C_2}\right), \tag{80}$$

$$(a_{33})_\infty = \left[\frac{1-C_2}{2-C_2}\left(\frac{S}{\Omega}\right) - 2\right](a_{22})_\infty + \frac{2}{3}\left(\frac{S}{\Omega}\right)\left(\frac{1-C_2}{2-C_2}\right), \tag{81}$$

where $(a_{22})_\infty$ is arbitrary.† Linear analysis also shows that this solution is an unstable saddle in the region $-0.0592 < \Omega/S < 0.3449$; numerical results indicate that this solution is actually unstable for the entire region $-0.0904 < \Omega/S < 0.3761$ where the alternative solution (73)–(78) is stable. The equilibrium solution (79)–(81) is a stable fixed point of the focus type for $\Omega/S < -0.0904$ and $\Omega/S > 0.3761$. Interestingly enough, there exists an additional branch of equilibrium solutions where $(\epsilon/SK)_\infty = 0$ and $(a_{12})_\infty$ is non-zero for $-0.0592 < \Omega/S < 0.3449$; however, these solutions are saddles which are, of course, unstable and thus never observable computationally. A bifurcation diagram of these equilibrium solutions for the LRR model is shown in figure 9 where we plot $(\epsilon/SK)_\infty$ *vs.* Ω/S. Only one stable equilibrium solution exists for a given value of Ω/S. It should be noted that the equilibrium solutions for which $(\epsilon/SK)_\infty > 0$ have a turbulent kinetic energy and dissipation rate that grow exponentially with time. The stable equilibrium solutions for which $(\epsilon/SK)_\infty = 0$ can have a turbulence structure that either grows or decays with time. More specifically, numerical solutions of the LRR model indicated an exponential growth in the turbulent kinetic energy and dissipation rate for $-0.11 \leqslant \Omega/S \leqslant 0.39$; there was a lower-law decay in the turbulent kinetic energy and dissipation rate for $\Omega/S < -0.11$ and $\Omega/S > 0.39$.

The RK model has equilibrium solutions of a similar nature. Non-zero values of

---

† Computations, however, indicate that for any given value of Ω/S only one value of $(a_{22})_\infty$ is stable.
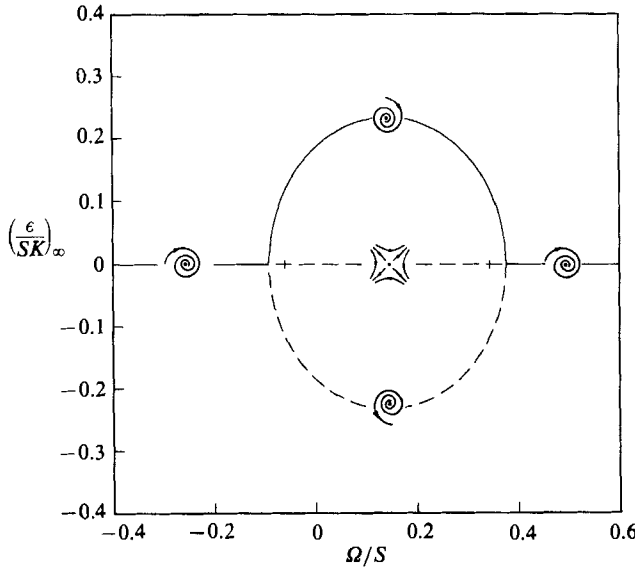
FIGURE 9. Bifurcation diagram for the LRR model.

$(\epsilon/SK)_\infty$ occur in the region $-0.0915 < \Omega/S < 0.5915$ for which the equilibrium states are given by

$$\left(\frac{\epsilon}{SK}\right)_\infty = \frac{\pm[\frac{1}{3}(1-B_1/6A_1)(1-3C_1)(E-3)-2C_1+8(\Omega/S)-16(\Omega/S)^2]^{\frac{1}{2}}}{B_1/6A_1-1-2/(E-3)}, \quad (82)$$

$$(a_{12})_\infty = \frac{2}{E-3}\left(\frac{\epsilon}{SK}\right)_\infty, \quad (83)$$

$$(a_{11})_\infty = \frac{4[\frac{2}{3}-2(\Omega/S)]}{(E-3)[1-B_1/6A_1+2/(E-3)]}, \quad (84)$$

$$(a_{22})_\infty = \frac{4[2(\Omega/S)-\frac{1}{3}]}{(E-3)[1-B_1/6A_1+2/(E-3)]}, \quad (85)$$

$$(a_{33})_\infty = \frac{-\frac{4}{3}}{(E-3)[1-B_1/6A_1+2/(E-3)]}, \quad (86)$$

where (as with the LRR model) analysis indicates that the positive branch $(\epsilon/SK)_\infty > 0$ is a stable fixed point of the focus type and the negative branch $(\epsilon/SK)_\infty < 0$ is an unstable fixed point of the same type. These branches of equilibria exist in conjunction with one where $(\epsilon/SK)_\infty = 0$ and $(a_{12})_\infty = 0$ which is valid for all Ω/S and given by

$$(\epsilon/SK)_\infty = 0, \quad (a_{12})_\infty = 0, \quad (87)$$

$$(a_{11})_\infty = \left(1-\frac{1}{2}\frac{S}{\Omega}\right)(a_{22})_\infty - \frac{1}{3}\frac{S}{\Omega}(1-3C_1), \quad (88)$$

$$(a_{33})_\infty = -\left(2-\frac{1}{2}\frac{S}{\Omega}\right)(a_{22})_\infty + \frac{1}{3}\frac{S}{\Omega}(1-3C_1), \quad (89)$$

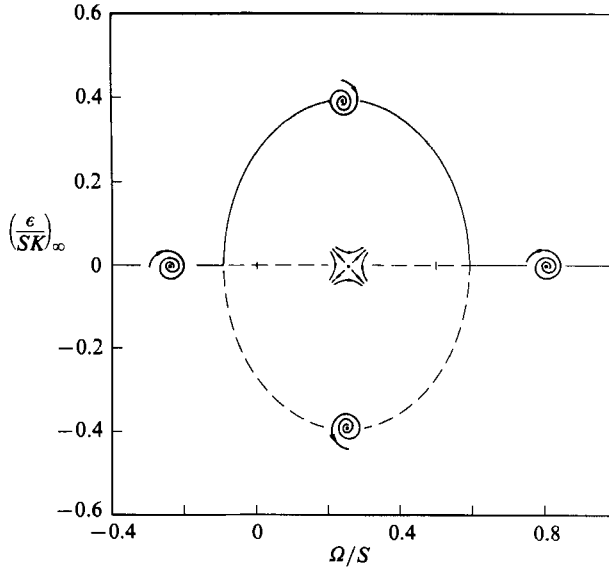where $(a_{22})_\infty$ can be arbitrary (computations, however, suggest that only one value

FIGURE 10. Bifurcation diagram for the RK model.

of $(a_{22})_\infty$ is stable for any given value of Ω/S). Computations indicate that the equilibrium solution (87)–(89) is unstable for $-0.0915 < \Omega/S < 0.5915$ (by a linear analysis it can be shown that (87)–(89) is an unstable saddle for $0.0009 < \Omega/S < 0.4991$). The stability of this solution for $\Omega/S > 0.5915$ and for $\Omega/S < -0.0915$ was verified by computations. It is interesting to note that (similar to the LRR model) the RK model has additional unstable equilibria where $(\epsilon/SK)_\infty = 0$ but $(a_{12})_\infty$ is non-zero in the region $0.0009 < \Omega/S < 0.4991$. By linear analysis, these equilibrium solutions can be shown to be saddles which are unstable. A bifurcation diagram for the RK model is shown in figure 10. It has the same structure as that for the LRR model (the two models are topologically equivalent from a dynamical systems standpoint). The primary difference between them is that the RK model predicts an equilibrium value of $(\epsilon/SK)_\infty = 0$ with a decaying turbulent kinetic energy and dissipation rate for $\Omega/S > 0.61$ as compared to the corresponding range of $\Omega/S > 0.39$ predicted by the LRR model. In this regard, the RK model is superior since large-eddy simulations and linear spectral models of turbulence suggest that rotating homogeneous shear flow is unstable for $0 \leqslant \Omega/S \leqslant 0.5$. While the LRR model is seriously in error in its prediction of a relaminarization for $0.39 < \Omega/S < 0.5$, it yields an equilibrium value for $(\epsilon/SK)_\infty$ that is in much better agreement with the pure shear experiments of Tavoularis & Corrsin (1981) than the result predicted by the RK model (see table 2). The fact that the LRR model deviates too strongly from Richardson-number similarity can be seen in the equilibrium values for the anisotropy tensor for $\Omega/S = 0.25$ shown in table 2. The LRR model predicts that $a_{22} \approx -3a_{11}$ whereas large-eddy simulations and supporting analogies with plane strain (see Bardina *et al.* 1983) indicate that $a_{11} \approx a_{22}$ as predicted by the RK model.

As alluded to earlier, it is not possible to obtain a closed-form solution for the equilibrium states of the SL model owing to its highly nonlinear nature. However, it was determined numerically that the SL model behaves similarly to the LRR model in that it predicts unstable flow for intermediate rotation rates in the range $-0.12 \leqslant \Omega/S \leqslant 0.40$; outside of this range the flow undergoes a relaminarization. The computed equilibrium states for the SL model are shown in table 2 along with those

Equilibrium values		LRR model	RK model	SL model	Experiments	Large-eddy simulations
$\Omega/S = 0$	a_{11}	0.381	0.483	0.228	0.403	0.61
	a_{22}	-0.190	-0.241	-0.232	-0.295	-0.53
	a_{12}	-0.369	-0.337	-0.243	-0.284	-0.29
	SK/ϵ	5.42	3.71	6.93	6.08	—
$\Omega/S = 0.25$	a_{11}	-0.119	0.121	-0.139	—	0.12
	a_{22}	0.310	0.121	0.134	—	0.09
	a_{12}	-0.415	-0.495	-0.305	—	-0.70
	SK/ϵ	4.83	2.53	5.51	—	—
$\Omega/S = 0.5$	a_{11}	-0.24	-0.241	-0.246	—	-0.53
	a_{22}	0.32	0.483	0.239	—	0.50
	a_{12}	0	-0.337	0	—	-0.20
	SK/ϵ	∞	3.71	∞	—	—

TABLE 2. Equilibrium results for homogeneous turbulent shear flow in a rotating frame: comparison of the predictions of the LRR, RK and SL models with the large-eddy simulations of Bardina *et al.* (1983) and the experiments of Tavoularis & Corrsin (1981).
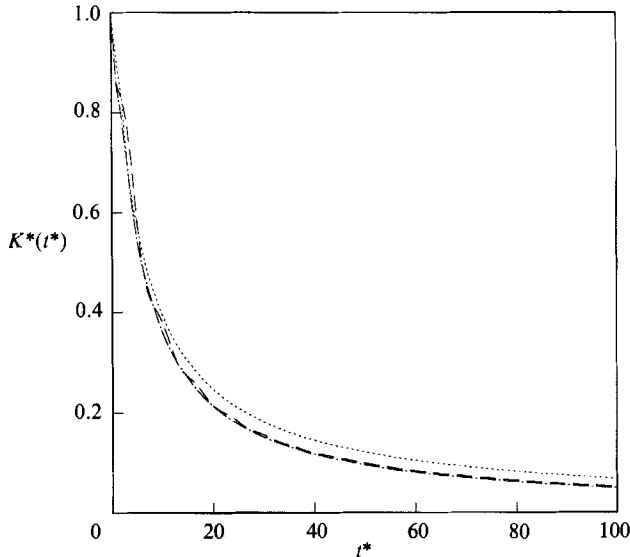

FIGURE 11. Time evolution of the turbulent kinetic energy for the second-order closure models: $\Omega/S = -0.25$, $\epsilon_0/SK_0 = 0.296$. Symbols as in figure 2.

discussed previously for the LRR model and the RK model. It is interesting to note that for $0 \leqslant \Omega/S \leqslant 0.5$ the predictions of the SL model are, on balance, no better than those for the LRR model which has a substantially simpler structure. A variety of initial conditions were shown to yield the same equilibrium states for the SL model as given in table 2. However, unlike the other models considered in this study, the equilibrium structure of the SL model is not universal (i.e. does not attract all initial conditions). It was found that some initial conditions for which $SK_0/\epsilon_0 \gg 1$ have no long-time solutions in the SL model owing to the function F in (62) turning negative (this causes the coefficient α_5 to become imaginary which terminates the computation). Finally, in regard to the SL model, some comments should be made concerning the sensitivity of the results to the constant $C_{\epsilon 1}^*$. A variety of values for
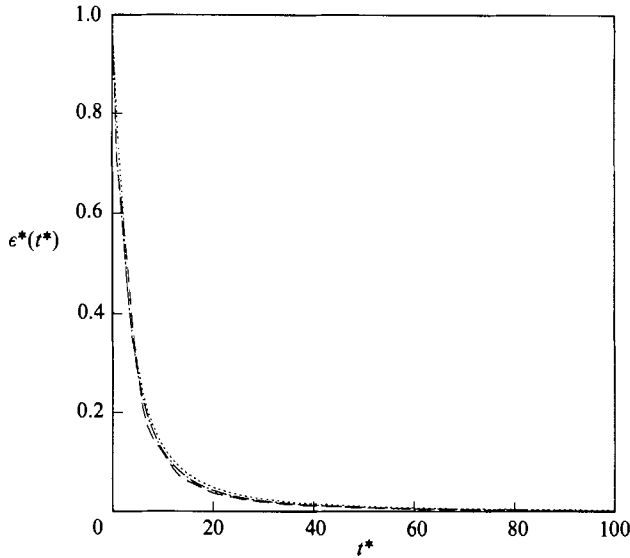
FIGURE 12. Time evolution of the turbulent dissipation rate for the second-order closure models: $\Omega/S = -0.25$, $\epsilon_0/SK_0 = 0.296$. Symbols as in figure 2.

$C_{\epsilon 1}^*$ ranging from 1.0 to 1.44 have been used (T. H. Shih 1988, private communication). The equilibrium values for SK/ϵ were found to be very sensitive to changes in $C_{\epsilon 1}^*$: for $C_{\epsilon 1}^* = 1.1$, $(SK/\epsilon)_\infty \approx 65$, whereas for $C_{\epsilon 1}^* = 1.44$, $(SK/\epsilon)_\infty = 6.93$. We decided to present results for $C_{\epsilon 1}^* = 1.44$ since this value is consistent with the K-ϵ model in the limit of small anisotropies and since it yields the best equilibrium values for SK/ϵ.

In figures 11 and 12, the time evolution of the turbulent kinetic energy and dissipation rate predicted by the various second-order closures is shown for $\Omega/S = -0.25$ and $\epsilon_0/SK_0 = 0.296$. For this counter-rotation, all of the second-order closures yield comparable results that are in good qualitative agreement with the linear spectral calculations of Bertoglio (1982) since they predict a strong, monotonic decay of the turbulent kinetic energy and dissipation rate.

In figure 13, the time evolution of SK/ϵ is shown for each of the models and for the direct numerical simulations of Lee, Kim & Moin (1987) corresponding to the case of strong shear with an initial condition of $SK_0/\epsilon_0 = 50$. The direct simulations were conducted using the Rogallo code which, for the weak shear case, was shown by Rogallo (1981) to yield equilibrium values of SK/ϵ in the range of those predicted by the turbulence models we have been considering. From figure 13, it is clear that the K-ϵ model, LRR model and RK model decrease monotonically to the same equilibrium values shown in table 2; the SL model also approaches the same equilibrium value as given on table 2 but more slowly and with oscillations (for $SK_0/\epsilon_0 > 100$, the function F in (62) turns negative and the SL model has no long-time solution). In contradiction to these model predictions, the direct simulations of Lee *et al.* (1987) indicate a monotonic growth of SK/ϵ (after a short initial period of decay) which suggests the possibility of an additional equilibrium solution for pure shear (where $(\epsilon/SK)_\infty = 0$) that attracts initial conditions for which $\epsilon_0/SK_0 \ll 1$. The recent experiments of Karnik & Tavoularis (1983) and Rohr *et al.* (1988) support the possibility of more than one fixed point in homogeneous turbulent shear flow. However, the issue still needs to be clarified.
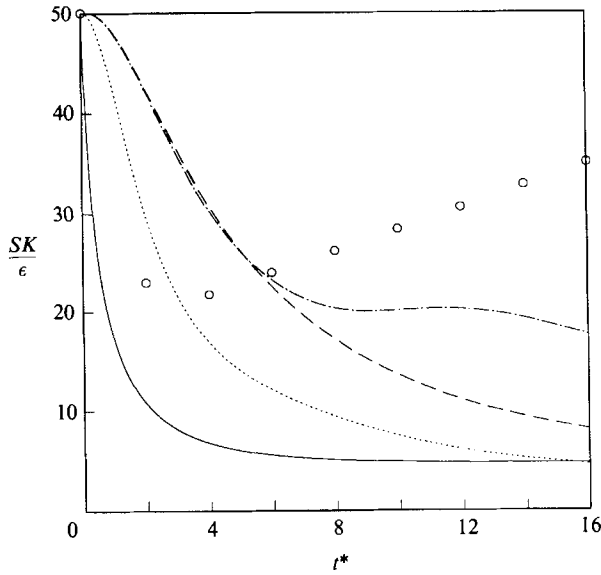
FIGURE 13. Time evolution of SK/ϵ for homogeneous turbulent shear flow ($\Omega/S = 0$, $SK_0/\epsilon_0 = 50$). ◯, Direct numerical simulations of Lee *et al.* (1987). Other symbols as in figure 2.
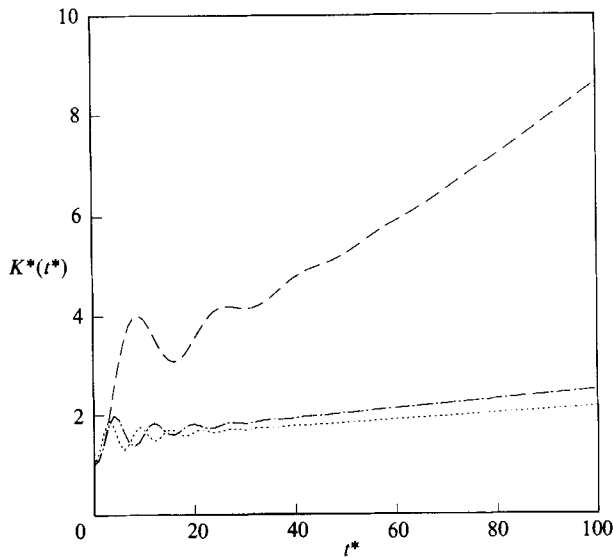

FIGURE 14. Time evolution of the turbulent kinetic energy for the second-order closure models: $\Omega/S = -0.1$, $SK_0/\epsilon_0 = 50$. Symbols as in figure 2.

The results shown in figure 13 suggest a potential problem concerning the applicability of the commonly used turbulence models to strong homogeneous turbulent shear flows. To further illustrate this point, the time evolution of the turbulent kinetic energy and dissipation rate are shown in figures 14 and 15, for the LRR, RK model and SL model corresponding to a mild counter-rotation of $\Omega/S = -0.1$ and a strong initial shear condition of $SK_0/\epsilon_0 = 50$. Both solutions are indicative of a monotonic growth in turbulent kinetic energy and dissipation with large-amplitude oscillations for $St < 50$. While one expects rotations to induce
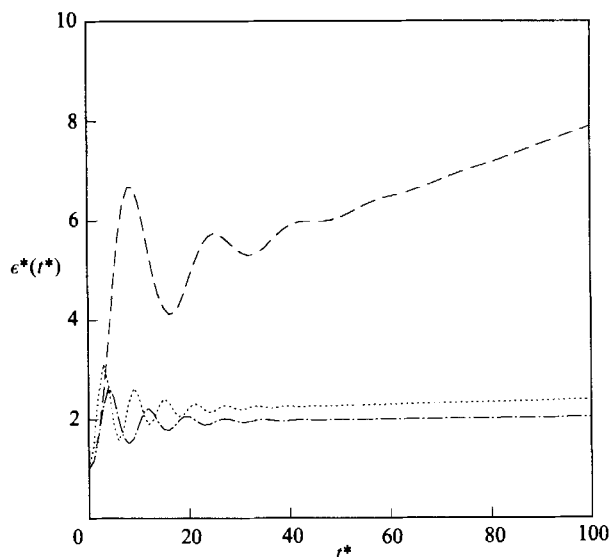
FIGURE 15. Time evolution of the turbulent dissipation rate for the second-order closure models: $\Omega/S = -0.1$, $SK_0/\epsilon_0 = 50$. Symbols as in figure 2.

inertial oscillations (and, consequently, it does seem to be correct that the models have fixed points of the focus type), it appears that the large amplitudes of the oscillations shown in figures 14 and 15 (particularly those of the LRR model) are unphysical. Such oscillations did not occur in the linear spectral calculations of Bertoglio (1982) for rotating shear flow and have not, to the best of our knowledge, been observed in any comparable flow configuration.

4. Conclusions

Five commonly used turbulence models have been tested for the problem of homogeneous turbulent shear flow in a rotating frame based on a dynamical systems analysis. Extensive comparisons between the predictions of the various models and the results of physical and numerical experiments have been made. The following definitive conclusions can be drawn:

(1) The standard K–ϵ model is highly deficient in that it yields solutions which are the same for all values of Ω/S, contrary to numerical simulations of the Navier–Stokes equations. In particular, the model substantially underpredicts the normal components of the anisotropy tensor for all values of Ω/S and does not account for the flow restabilization that occurs for most positive Richardson numbers.

(2) The nonlinear K–ϵ model yields improved predictions for the normal components of the anisotropy tensor that are in the correct range of the results of large-eddy simulations for $0 \leqslant \Omega/S \leqslant 0.5$ and physical experiments for $\Omega/S = 0$. However, the nonlinear model yields the same deficient predictions for K and ϵ as the standard K–ϵ model.

(3) The Launder, Reece & Rodi model yields reasonably acceptable predictions for the time evolution and equilibrium states corresponding to pure shear ($\Omega/S = 0$). However, the quality of the predictions degrades considerably with increasing Ω/S in the unstable flow regime. The model erroneously predicts flow restabilization for

negative Richardson numbers (i.e. for $0.39 < \Omega/S < 0.5$, $-0.17 < Ri < 0$). Furthermore, for strong initial shear rates where $SK_0/\epsilon_0 \gg 1$, the model can give rise to large-amplitude inertial oscillations which appear to be unphysical.

(4) The Rotta–Kolmogorov model predicts unstable flow (i.e. unbounded growth in K and ϵ) for $-0.11 \leqslant \Omega/S \leqslant 0.61$ which is in reasonable agreement with numerical simulations and linear spectral analyses of the Navier–Stokes equations. Its predictions for the equilibrium anisotropy tensor are moderately good (except for a_{33} which is erroneously independent of Ω/S), but it yields poor quantitative results for the equilibrium values of SK/ϵ and gives rise to points of inflection and large-amplitude inertial oscillations for some time evolutions of K and ϵ. The model exhibits exact similitude with respect to the Richardson number which is not supported by large-eddy simulations. Nevertheless, in this regard, it is still superior to the LRR model which deviates too strongly from Richardson-number similarity in its prediction of a premature relaminarization.

(5) The Shih–Lumley model is not energetic enough and consistently underpredicts the kinetic energy and dissipation rate in the unstable flow regime $0 \leqslant \Omega/S \leqslant 0.5$. Unfortunately, its predictions for the equilibrium states are no better than those of the older second-order closures (i.e. the LRR model and the RK model) which have a considerably simpler structure. Like the LRR model, it deviates too strongly from Richardson-number similarity in its erroneous prediction of flow restabilization for negative Richardson numbers (i.e. for $-0.15 \leqslant Ri < 0$). Furthermore, it has no long-time solutions for certain initial conditions corresponding to strong shear where $SK_0/\epsilon_0 \gg 1$.

Finally, we shall make suggestions for the development of improved models. It is clear that the major deficiency with the nonlinear K–ϵ model lies in its lack of an $(\epsilon/SK)_\infty = 0$ fixed point and the lack of any dependence on Ω/S in the dissipation rate transport equation. This can be corrected by allowing $C_{\epsilon 1}$ and $C_{\epsilon 2}$ to be nonlinear functions of an appropriate flow invariant which reduces to $\epsilon/\Omega K$ for rotating shear flow. With such a correction, the nonlinear K–ϵ model could become a strong competitor to the commonly used second-order closure models. In order to improve the second-order closures, we propose that material frame-indifference in the limit of two-dimensional turbulence (which constitutes a geostrophic flow constraint that all of the models considered herein violate) be applied in the manner of Haworth & Pope (1986) and Speziale (1985). This should yield improved behaviour in the low-Rossby-number limit and provide the possibility of an additional fixed point for the high-shear-rate case since this correction increases by one the degree of the nonlinearity in τ_{ij}. The implementation of these improvements and their evaluation based on a dynamical systems approach will be the subject of future work.

REFERENCES

BARDINA, J., FERZIGER, J. H. & REYNOLDS, W. C. 1983 Improved turbulence models based on large-eddy simulation of homogeneous, incompressible turbulent flows. *Stanford University Tech. Rep. TF-19.*

BERTOGLIO, J. P. 1982 Homogeneous turbulent field within a rotating frame. *AIAA J.* **20**, 1175–1181.

CHAMPAGNE, F. H., HARRIS, V. G. & CORRSIN, S. 1970 Experiments on nearly homogeneous turbulent shear flow. *J. Fluid Mech.* **41**, 81–139.

HANJALIC, K. & LAUNDER, B. E. 1972 A Reynolds stress model of turbulence and its application to thin shear flows. *J. Fluid Mech.* **52**, 609–638.

HAWORTH, D. C. & POPE, S. B. 1986 A generalized Langevin model for turbulent flows. *Phys. Fluids* **29**, 387–405.

KARNIK, V. & TAVOULARIS, S. 1983 The asymptotic development of nearly homogeneous turbulent shear flow. In *Turbulent Shear Flows*, vol. 4 (ed. L. J. S. Bradbury, F. Durst, B. E. Launder, F. W. Schmidt & J. H. Whitelaw), pp. 14.18–14.22. Springer.

LAUNDER, B. E., REECE, G. & RODI, W. 1975 Progress in the development of a Reynolds stress turbulence closure. *J. Fluid Mech.* **68**, 537–566.

LEE, M. J., KIM, J. & MOIN, P. 1987 Turbulence structure at high shear rate. In *Proc. Sixth Symp. on Turbulent Shear Flows, Toulouse, France*, pp. 22.6.1–22.6.6.

LUMLEY, J. L. 1978 Turbulence modeling. *Adv. Appl. Mech.* **18**, 123–176.

MELLOR, G. L. & HERRING, H. J. 1973 A survey of mean turbulent field closure models. *AIAA J.* **11**, 590–599.

MELLOR, G. L. & YAMADA, T. 1974 A hierarchy of turbulence closure models for planetary boundary layers. *J. Atmos. Sci.* **31**, 1791–1806.

PATERA, A. T. & ORSZAG, S. A. 1981 Finite-amplitude stability of axisymmetric pipe flow. *J. Fluid Mech.* **112**, 467–474.

REYNOLDS, W. C. 1987 Fundamentals of turbulence for turbulence modeling and simulation. *Lecture Notes for Von Karman Institute, AGARD Rep.* 755. NATO.

RODI, W. 1972 The prediction of free turbulent boundary layers by use of a two-equation model of turbulence. Ph.D. thesis, University of London.

ROGALLO, R. S. 1981 Numerical experiments in homogeneous turbulence. *NASA Tech. Mem.* 81315.

ROHR, J. J., ITSWEIRE, E. C., HELLAND, K. N. & VAN ATTA, C. W. 1988 An investigation of the growth of turbulence in a uniform mean shear flow. *J. Fluid Mech.* **187**, 1–33.

SHIH, T. H. & LUMLEY, J. L. 1985 Modeling of pressure correlation terms in Reynolds stress and scalar flux equations. *Tech. Rep. FDA-85-3.* Cornell University.

SPEZIALE, C. G. 1985 Second-order closure models for rotating turbulent flows. *ICASE Rep. 85-49.* NASA Langley Research Center.

SPEZIALE, C. G. 1987 On nonlinear K–l and K–ϵ models of turbulence. *J. Fluid Mech.* **178**, 459–475.

SPEZIALE, C. G. 1989 Turbulence modeling in non-inertial frames of reference. *Theor. Comp. Fluid Dyn.* **1**, 3–19.

SPEZIALE, C. G. & MAC GIOLLA MHUIRIS, N. 1989 Scaling laws for homogeneous turbulent shear flows in a rotating frame. *Phys. Fluids* A **1**, 294–301.

TAVOULARIS, S. 1985 Asymptotic laws for transversely homogeneous turbulent shear flows. *Phys. Fluids* **28**, 999–1004.

TAVOULARIS, S. & CORRSIN, S. 1981 Experiments in nearly homogeneous turbulent shear flows with a uniform mean temperature gradient. Part 1. *J. Fluid Mech.* **104**, 311–347.

TRITTON, D. J. 1977 *Physical Fluid Dynamics.* Van Nostrand.

TUCKER, H. J. & REYNOLDS, A. J. 1968 The distortion of turbulence by irrotational plane strain. *J. Fluid Mech.* **32**, 657–673.